Hidden effects of negative stacking fault energies in complex concentrated alloys

Zongrui Pei¹, Biswanath Dutta², Fritz Körmann^{2,3} and Mingwei Chen⁴

¹Oak Ridge National Laboratory, Oak Ridge, Tennessee 37831, USA

²Department of Materials Science and Engineering,
Faculty of Mechanical, Maritime and Materials Engineering,
Delft University of Technology, Mekelweg 2, 2628 CD Delft, The Netherlands

³Computational Materials Design, Max-Planck-Institut für Eisenforschung GmbH, D-40237 Düsseldorf, Germany and

⁴Department of Materials Science and Engineering and Hopkins Extreme Materials Institute,
Johns Hopkins University, Baltimore, Maryland 21218, USA

(Dated: May 10, 2021)

Negative stacking fault energies (SFEs) are found in face-centered cubic high-entropy alloys with excellent mechanical properties, especially at low temperatures. Their roles remain elusive due to the lack of *in situ* observation of nanoscale deformation. Here the polymorphism of Shockley partials is fully explored, assisted by a new method. We show negative SFEs result in novel partial pairs as if they were in hexagonal close-packed alloys. The associated yield stresses are much higher than other mechanisms at low temperatures. This generalizes the physical picture for all negative-SFE alloys.

Low to negative stacking fault energies (SFEs) are frequently found for high-entropy alloys (HEAs) in theory, particularly for the alloys with excellent mechanical properties, such as CoCrFeNiMn [1-4] and CoCrNi [5-9]. Negative SFEs are difficult to be identified in experiment, but their existence is indicated by the rich twin and various close-packed nanostructures [10]. In theory, Ising models connect the negative SFE with the lower energy of hexagonal close-packed (hcp) structure relative to face-centered cubic (fcc) [11]. For example, the hcp Cantor alloy (CoCrFeNiMn) is indeed thermodynamically more stable than the fcc one at cryogenic temperatures [12]. Alloys are usually synthesized at high temperatures when fcc structure is more stable than hcp, and then quenched down to room or cryogenic temperatures when the stability is probably reversed. The phase transition from fcc to hcp can be kinetically too slow to see. However, the hcp phases under high pressures indeed formed and retained in CoCrFeNiMn [13, 14] and CoCr-FeNi [15] even when the pressures were removed. It is widely acknowledged that low to negative SFEs usually result in wide stacking faults (SFs) and large distance between partial dislocations. The mechanical implications of low SFE have been studied [16, 17], but those of negative SFE are still elusive and urgently need further experimental [18] and theoretical explorations. Partial dislocations can shape the microstructure and mechanical properties of fcc materials. The abundant Shockley partials and their polymorphism in these HEAs request all intrinsic geometric freedoms for a complete description of dislocation geometry. Here we propose a new notation system that can unambiguously describe all possible dislocation geometries. Assisted by it, our theoretical analysis shows large width of SFs is not the only effect of negative SFEs, but one of them. The other consequences include a novel dislocation geometry similar to a dissociated dislocation in hcp structure (Figure 1c-d, Case C), where the two partials switch their positions in Case O. It is similar to the Lomer-Cottrell lock but with partials

on the same slip plane. The special situation of Case C, i.e., when the coupled partials are far away, is profuse in fcc materials with negative SFEs including HEAs. It is fundamentally interesting to check whether this new mechanism plays a role in the excellent mechanical properties of HEAs. This mechanistic study is based on a new density functional theory (DFT)-informed multiple-equal-fraction-dislocation (MEFD) formulation [19] and two solute solution strengthening models [16, 17]. From the general point of view, Case C is still special in the large possibility space when the constraints associated with positive SFEs are removed.

Full exploration for novel dislocation geometry by a new notation system The extremely plentiful configurations of the partials are exemplified by CoCrNi [20, 21], CoCrFeNiMn [20] and Al0.1CoCrFeNi [22] in Figure 1a. Their geometries cannot be definitely described by Burgers vector only, where the positions of SFs relative to the partials are ignored. This text-book notation system works well for alloys of positive SFEs, since the relative positions of two partials and one SF are always well defined. Problems arise when partials are abundant and unbound when SFEs are extremely low to negative. Two partials under observation can be separated by the fcc matrix rather than a SF. When SFEs are negative the two partials can even be bound together by the fcc matrix. There are three intrinsic geometric freedoms needed for a definite description of arbitrary number of partials: (i) Burgers vectors \vec{b}_i ; (ii) line directions \vec{s}_i ; and (iii) the position of partials relative to SFs. The choice of Burgers vectors is described by the Thompson's tetrahedron; the line direction is in principle arbitrary if symmetry permits; both can be clearly described by the text-book notation system. However the relative positions of the partials is not defined, which is indispensable for alloys with negative SFEs.

A new notation system is proposed here for a complete description of the extremely diverse dislocation geometries (Figure 1b). The new symbol combines the Burgers

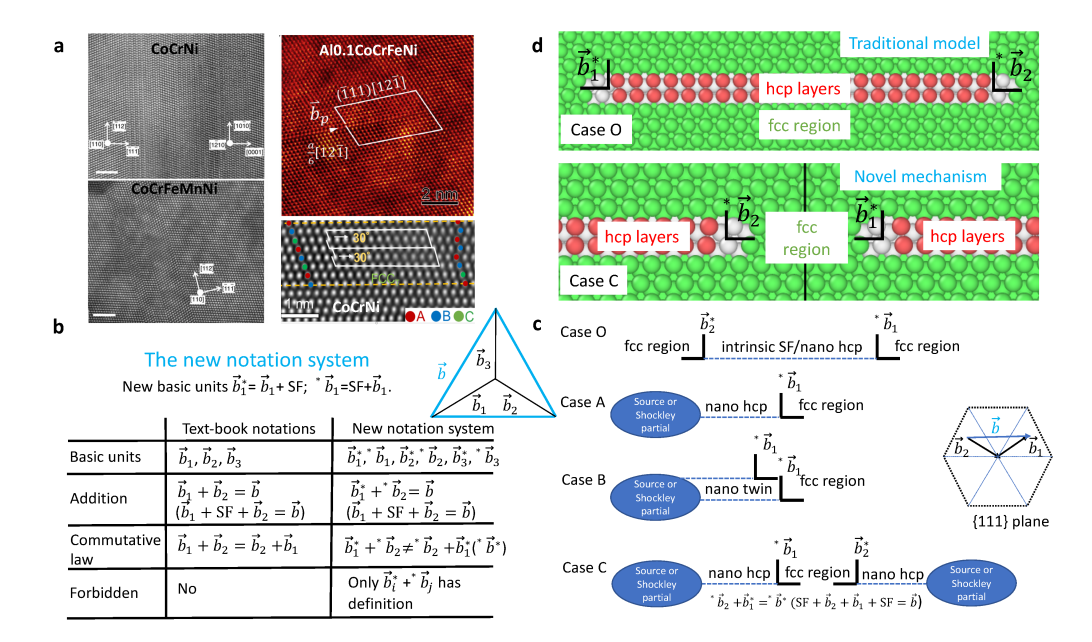


FIG. 1: Full exploration for novel dislocation geometry by a new notation system. **a**, Nanoscale close-packed stackings formed by partial dislocation motions are exemplified by CoCrNi [20, 21], CoCrFeNiMn [20] and Al_{0.1}CoCrFeNi [22]. The profuse partials are highlighted. **b**, The new notation system and its comparison with the text-book notion. **c**, Four possible configurations of Shockley partials in fcc concentrated alloys. The partials have typical Burgers vectors $\vec{b}_1 = 1/6[1\bar{2}1]$, and $\vec{b}_2 = 1/6[2\bar{1}1]$. The blue arrows indicate the Burgers vectors of Shockley partials. **d**, The configurations of Case C and Case O are illustrated with atomic resolution. The red region consists of two hcp layers, and the green region is the fcc matrix.

vector of a partial and the SF position. For example, when a SF is to the right of the partial \vec{b}_1 , we denote it by \vec{b}_1^* , $\vec{b}_1^* = \vec{b}_1$ +SF; when it is to the left, $^*\vec{b}_1 = \text{SF} + \vec{b}_1$. The properties of the new notation system and its applications to describe cases in Figure 1c and beyond are referred to the supplementary material. The new system considers all intrinsic geometric freedoms in a simple manner, but the impact is profound. It is useful to describe more complex geometry, where three or more partial dislocations are involved. The line direction \vec{s} is arbitrary in theory. A general discussion of arbitrary directions is straightforward but outside the scope of this work. Here we only consider the two partials with the same line direction. The new notation system can help explore novel configurations of the Shockley partials.

The new building blocks of starred Burgers vectors (partials) double in number, which greatly increases the possibilities of combinations of partials. We can mechanically play the building blocks to find new geometry and then check if they can be a new mechanism with physical meaning. Arguably the most easy way to find a new geometry is to switch the positions of partials in known configurations. For example, we can switch the two partials in Case A, which results in Case C (Figure 1c). This is similar to a dissociated dislocation in hcp structure, which can exist in alloys with negative SFEs. As a new type of dislocation geometry in fcc, it provides the basis to understand deformation behavior. Its special situation when the coupled partials are far away and behave like independent partials in non-equilibrium state, is profuse

in fcc materials with negative SFEs including HEAs. As examples, the geometry and mechanics of Case C are discussed as a novel mechanism for two typical HEAs, i.e., CoCrFeNiMn [13, 14] and CoCrFeNi [15].

The broken equilibrium: Case O In the classic Case O, three forces determine the distance between the two Shockley partials, i.e., the interactions of edge components $F_e(x)$, screw components $F_s(x)$ and the attractive force through SFEs $F_{\gamma}(x)$. Assuming \vec{b}_1^* , $^*\vec{b}_2$ are the Burgers vectors of the two partial dislocations, \vec{s} is the line direction of the whole dislocation, G is the shear modulus along the Burgers vector \vec{b} of the whole dislocation, ν is the Poison ratio, we have $F_e = \frac{G}{2\pi(1-\nu)}\frac{1}{x}(\vec{b}_1^*\times\vec{s})(^*\vec{b}_2\times\vec{s}) > 0$, $F_s = \frac{G}{2\pi}\frac{1}{x}(\vec{b}_1^*\cdot\vec{s})(^*\vec{b}_2\cdot\vec{s}) < 0$, and $F_{\gamma} = -x\gamma_0 < 0$. Here γ_0 represents the SFE. The equilibrium distance x_0 is calculated by

$$F_e(x_0) + F_s(x_0) + F_\gamma(x_0) = 0. (1)$$

When the SFE is negative, i.e., $F_{\gamma} = -x\gamma_0 > 0$, the force associated with SFE becomes repulsive and has the same sign as F_e . The equilibrium of Eq. 1 is however broken. The only attractive force F_s from the screw components is smaller than F_e let alone there is an extra repulsive force term from SFE. The total force is thus

$$F_e(x) + F_s(x) + F_{\gamma}(x) > 0.$$
 (2)

Obviously there is no solution for x. We will confirm this information again from the numerical solution of one revised Peierls-Nabarro model.

When Shockley partials are profuse, it is also possible that one of the partials has a pure screw character. For example, when the right partial is purely screw with SF to its left (* \vec{b}_3), $F_e = 0$, we can find a new equilibrium distance $x_0 = -F_s/\gamma_0$. An equivalent case is the left partial is a screw dislocation, which yields the same equilibrium distance. Here we focus on a special case, i.e., when the two partials have mixed characters but meet each other from an opposite direction.

The new equilibrium: Case C According to classic dislocation theory [23–25], the perfect dislocation can never be nucleated due to their large critical resolved shear stress (CRSS) during nucleation τ_N . Instead many twins and SFs are formed because of the lower CRSS τ_p to nucleate Shockley partial dislocations. $\tau_N = \frac{2\alpha_0 Gb}{D}, \tau_P = \frac{2\alpha_0 Gb_1}{D} + \frac{\gamma_0}{b_1}$. Here parameter α_0 is a constant for either edge or screw dislocation. When $\gamma_0 < 0$, τ_N is always smaller than τ_P , regardless of grain size D. The huge amount of partials may meet each other and form new couples in the configuration of Case C (Figure 1c-d, Case C), which can be expressed by $*\vec{b}_1 + \vec{b}_2^* = *\vec{b}^*$.

The configuration of Case C is similar to the dissociated basal $\langle a \rangle$ dislocation on the basal plane in hcp if the principle of nearsightedness is adopted. Transforming the Case C in fcc into the hcp basal $\langle a \rangle$ dislocation where the bulk hcp energy as the new zero energy reference, we again have a positive SFE and the associated force $F_{\gamma}=-x\gamma_0<0$. The new equilibrium distance would be $x_0=\frac{Gb}{\gamma_0}\frac{b}{24\pi}\frac{2+\nu}{1-\nu}$ (consequence of Eq. 1). Different from Case O, here the shear modulus G and Poisson ratio ν of hcp rather than fcc are needed, assuming that a dislocation can only feel the interactions of its nearestneighbor layers. This assumption has been adopted for dislocation-solution interactions [26, 27]. Poisson ratios of both hcp and fcc structures are stably close to 0.3, particularly for the materials with the same constitutions and crystal structures. With the above preparation Case C in fcc materials can be transformed into Case O in hcp ones. The great advantage of this transformation is, (i) the minus sign of SFE can be dropped and (ii) the dislocation geometry of Case C can be evaluated by classic dislocation theory.

Higher yield stresses in Case C indicated by GSFEs Generalized SFE (GSFE) is a very useful concept associated with SFE that provides insights into the mechanical properties. Accurate GSFEs are calculated by DFT (Figure 2), which can be used to fit the five-point γ surface [28] or its simplified two-point expression, $\gamma(x) = \gamma_0 \sin^2(\pi x) + (\gamma_u - \gamma_0/2) \sin^2(2\pi x)$, where γ_0, γ_u are the stable and unstable SFEs. This expression can be easily used to evaluate the effect of SFE on dislocation geometry and strengthening. Also the shear modulus can be well evaluated by the slops of GSFE curves, which are substantially different for hcp and fcc [12]. For Case O, a Shockley partial has to overcome the barrier along the direction x = 0 to 1/4; while for Case C, a larger barrier

of the reversed direction has to be overcome. The GSFE curves of hcp and fcc show that the "valley" is deeper for hcp partials than fcc one (arrows in Figure 2), indicating a larger CRSS of Case C than Case O.

The γ surface or GSFE curve is reconstructed for Case C. Two steps are needed: (i) drop the minus sign of SFE; (ii) add SFE to the unstable SFEs γ_u . Step (i) is based on ANNNI models, which state the SFEs for intrinsic SF I₁ in hcp [29] and the intrinsic SF in fcc are

$$\gamma_{\text{hcp}} \approx -4J_1 + 4J_2 - 4J_3 \approx -4J_1 - 4J_3,$$
 (3a)

$$\gamma_{\rm fcc} \approx 4J_1 + 4J_3 \approx -\gamma_{\rm hcp}.$$
 (3b)

The extensive data of Hu et al. shows J_2 is about $J_1/10$ to $J_1/3$ [30]. As a reasonable approximation, $\gamma_{\rm hcp} \approx -\gamma_{\rm fcc}$. This results in two coupled correspondences, i.e., (i) negative SFE in hcp corresponds to a positive one in fcc and (ii) negative SFE in fcc corresponds to a positive one in hcp. The above idea allows us to treat a fcc problem with a negative SFE as a hcp one with a positive SFE. This finding directly attributes the different yield stresses of Cases O and C to the different shear moduli of fcc and hcp phases.

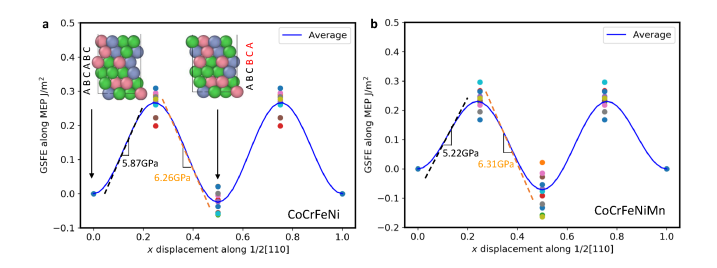


FIG. 2: The minimum energy paths (MEPs) for dislocation motions. a MEPs of GSFEs for CoCrFeNi (left) and b CoCrFeNiMn (right). The insets in (a) illustrate the atomic arrangements before and after Shockley partial glides, the geometries of which are the same for CoCrFeNiMn albeit with different atomic occupations. For both alloys the maximum shear stress in Case C (right slope, dashed line in yellow) is larger than in Case O (left slope, dashed line in black), indicating a higher yield stress of Case C than the classic one.

Dislocation geometry by MEFD calculations It is not convenient to simulate the atomic structure of Case C using atomistic simulations or DFT, since the fcc matrix is less stable than hcp at zero K. We use a revised Peierls-Nabarro model with the MEFD formulation for this purpose. This model yields the key parameters to describe the dislocation geometry, i.e., the distance between the partials and their half widths. The most important input for the model is the γ surface introduced in the preceding section. The MEFD formulation is used to solve the equation [19], which has been successfully used to study Mg [19], HEAs [33] and two-dimensional materials [34]. A total of seven parameters are optimized using the Particle Swarm Optimization (PSO) algorithm [11, 28, 35] that have been implemented in DIST toolkit [36].

Figure 3 shows the optimized dislocation core geometry using DFT-computed GSFEs and elastic constants. The core structures in the new Case C are different from that in the classic Case O, due to the dominant attractive interaction between partials. In Case O, the interaction is either negligible or repulsive. The geometric difference is more significant in Cantor alloy than in CoCrFeNi. For Cantor alloy, the half-width w of each partial in Case C is slightly wider than that in Case O. The equilibrium distance between partials for both alloys in Case C is about 8.5 Burgers vector; while for Case O, the distance is theoretically infinite, consistent with the classic analytical model.

There is lack of direct observations for the equilibrium geometry of Case C in Figure 3. There are multiple reasons for it. Firstly, few experimentalists notice this novel configuration of partials, so they do not have the motivation to find it. The new notation system and our theoretical treatment of the new dislocation geometry will make a change. Secondly, Case C is not a lock but mobile. They can only be stopped by other defects (e.g., grain boundaries), which is either difficult to identify or simply outside the limited observation field of microscopes. A similar the technical challenge is that it may require a large-scale atomic observations to confirm two widely separated partials on the same atomic plane. In addition, there are also possible reasons from viewpoints of thermodynamics and kinetics, which we do not elaborate here. Nonetheless, Case C still can provide the basis to understand the mechanical behavior of alloys with abundant partials. Its non-equilibrium state of partial distance $d \to +\infty$ is equivalent to the experimentally observed partials (Figure 1a), which will be discussed below.

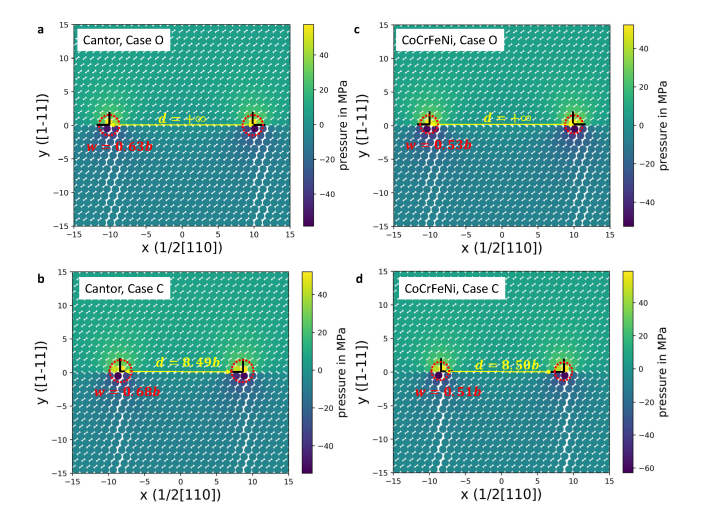


FIG. 3: The dislocation cores computed by a revised Peierls-Nabarro model. Both the classic (\mathbf{a}, \mathbf{c}) and new (\mathbf{b}, \mathbf{d}) configurations of Shockley partials in the Cantor and CoCrFeNi alloys are calculated. The partial distance of the classic configuration (Case O) is theoretically infinite, which is reset as 10b for better visualization.

Mechanical consequences of the novel mechanism and magnetic states The GSFE curves indicate Case C has a higher CRSS than the classic Case O. Here we directly evaluate their mobility using two widely accepted models. The influence of magnetic states, which are sensitive to the local arrangements of the close-packed planes, is also discussed. Okamoto et al. [17] found that the yield stress normalized by shear modulus G for a given alloy follows a rule $\sigma_y/G = k \cdot \text{MSAD}^{1/2}$, where $k \approx$ 1.3×10^{-3} MPa/pm for fcc HEAs, and MSAD represents the mean square atomic displacement. For example, MSAD^{1/2}=4.8 pm, $\sigma_y/G = 6.21 \times 10^{-3}$ for Cantor alloy; for CoCrFeNi, MSAD $^{1/2}$ =5.46 pm, $\sigma_y/G = 7.10 \times 10^{-3}$. The rule can be recast into $\sigma_y/(k \cdot \text{MSAD}^{1/2}) = G$. For different cases (O, C) and different magnetic states, G or equivalently $\sigma_y/(k\cdot \text{MSAD}^{1/2})$ is different. Three different magnetic states (such as paramagnetism, antiferromagnetism, etc.) are simulated for fcc and hcp bulk moduli by DFT at 0K. Computational details are referred to the supplementary material. The shear moduli G are calculated by bulk moduli and a Poisson ratio of 0.3. The rescaled yield stresses $\sigma_v/(k \cdot \text{MSAD}^{1/2})$ for the 6 different situations are shown in Figure 4. The magnetic states substantially change the rescaled yield stresses in both Cases O and C. The most significant feature is that Case C (A2,B2,C2) offers a much higher yield stresses than Case O (A1,B1,C1) for the Cantor alloy; while the experimental value lies in between. In contrast, the yield stresses for the CoCrFeNi alloy in Cases O and C are less different and comparable to the influence of the magnetic states. The strengthening effect of magnetism was discussed [20]. Here we directly quantified the its effect on yield stresses.

We consider a special situation of Case C when the two partials are far away, which is profuse in experiment (Figure 1a). The Varvenne model is derived for exactly this situation [16] and can be adopted to calculate yield stresses above 0K. The model is a revised version of the solute solution strengthening model proposed by Leyson [26] and were demonstrated to have quantitative predictability [9, 37]. The model and its connection with the Okamoto model was discussed by Nohring $et\ al.\ [38]$ We do not describe the full details available in the references and just show the formula to calculate τ at 0K, i.e.,

$$\sigma_y = 0.051 M \alpha^{-\frac{1}{3}} K_{\tau} f_{\tau} \left[\sum_n c_n \Delta V_n^2 \right]^{\frac{2}{3}}$$
. Here M is the Taylor factor of 3.06, the line tension constant $\alpha = 0.123$ and the geometric constant for wide-core dislocation $f_{\tau} = 0.35$ and elasatic constant $K_{\tau} = \bar{G} (\frac{1+\bar{\nu}}{1-\bar{\nu}})^{4/3} b^{-4}$. The key parameter is the total volume misfit $\sum_n c_n \Delta V_n^2$ with all elements considered at the same footing. Together with another energy term, the finite-temperature τ is determined through an Arrhenius-type function.

The temperature-dependent yield stresses are calculated for the new mechanism (Case C) in two HEAs (Figure 4). The new mechanism indeed provides a much larger yield stress than the classic mechanism (Case O)

for CoCrFeNiMn. At cryogenic temperatures, a 50% higher yield stress is predicted for Case C (paramagnetic state), which better agrees with the experimental measurement for the alloy. This gives another effect induced by the negative SFEs in the HEA, which is *intrinsic* to the new Shockley pairs. The yield stress is more affected by the different mechanisms but also substantially tuned by the magnetic states. For example, the yield stress of paramagnetic state is larger than the other two states in Case C. In contrast, the variance of yield stress due to the new mechanism is comparable to the magnetic states for CoCrFeNi. Further experimental investigations on the probability or density of the new configuration (Case C) are still needed.

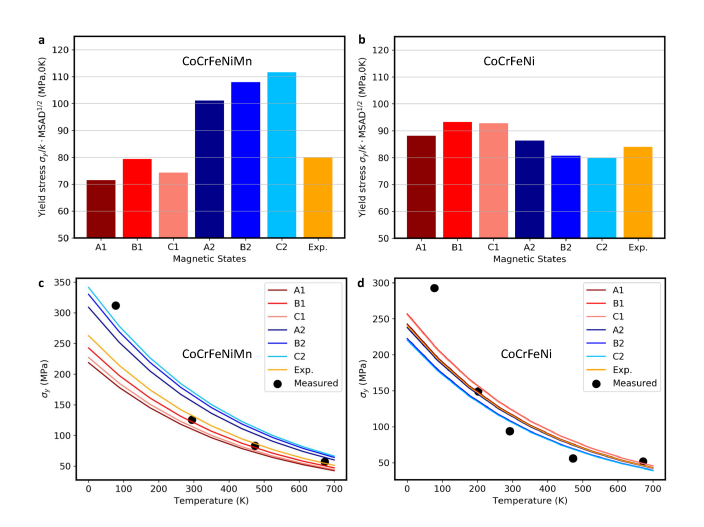


FIG. 4: The mechanical consequences of the new mechanism. The magnetic-state dependent yield stresses for the new and classic configurations of dislocations, i.e., yield stresses at zero K (\mathbf{a} - \mathbf{b}) and at finite temperatures (\mathbf{c} - \mathbf{d}). The letters represent magnetic states and numbers are for different cases (O/C). A: Ferrimagnetic, B: Antiferromagnetic, C: Paramagnetic; 1-Case O; 2-Case C. Both measured yield stresses (dots) and calculated ones using experimental elastic constants (yellow line, exp.) are presented.

In addition to alloy yielding, the new mechanism can also affect the strain hardening through screw dislocations, another important topic in HEAs [39–42]. When the Shockley partials form a new pair, the recombination of the original partials into a whole dislocation with a geometry of Case O is prohibitively difficult. Each partial has to overcome the energy barriers to break with the partners in the configuration C to recover Case O. This

can reduce the number of available screw dislocations that cross slip and eventually affect the strain hardening rate. The classic Taylor model connects the strain hardening directly with the available dislocation density [43], $\Delta\sigma = \beta Gb\sqrt{\rho}, \text{ where } \beta \text{ is a constant depending on the interactions of dislocations, } \rho \text{ is the dislocation density.}$ Case C helps increase ρ as well as the ultimate strength. Another closely related topic is to investigate how Case C affects the serration phenomena at cryogenic temperature in HEAs, which is well-known for the Cantor alloy [44].

In summary, we fully explore the geometric and mechanical implications of negative SFEs in high-entropy alloys and add fundamentally new ingredients to understand their excellent mechanical properties. We identify a new dislocation geometry assisted by a notation system invented here. The new configuration of Shockley partials and its special case are expected to be found for all alloys with negative SFEs, which are systematically studied using state-of-the-art DFT simulations and multi-scale models, and compared with available experimental measurements. The new dislocation geometry results in a higher yield stress at cryogenic temperatures than the traditional mechanisms for CoCrFeNiMn and agrees better with the experiment, which can be activated below the cross-over temperature of the fcc and hcp free energies. The interplay between the new mechanism and various magnetic states of atoms is directly evaluated, showing that magnetism can substantially tune the magnitudes of yield stresses. In addition to yielding, other mechanical consequences are also discussed. Our study demonstrates negative SFEs provide a new group of mechanisms, in addition to the known effects, such as wide SFs. This generalizes the physical picture and lays the foundation for the design of all novel negative-SFE alloys.

This work was sponsored by the U.S. Department of Energy, Office of Science, Basic Energy Sciences, Materials Science and Engineering Division. This research used resources of the Oak Ridge Leadership Computing Facility, which is supported by the Office of Science of the U.S. Department of Energy under Contract No. DE-AC05-00OR22725. B.D. and F.K. gratefully acknowledge funding from the Deutsche Forschungsgemeinschaft (SPP 2006) and from NWO/STW (VIDI Grant No. 15707). M.C. acknowledges the support of U.S. National Science Foundation under grant DMR-1804320. The authors also acknowledge the fruitful discussion with Dr. Duancheng Ma and Dr. Hongwei Sheng.

B. Cantor, I. Chang, P. Knight, A. Vincent, Microstructural development in equiatomic multicomponent alloys, Materials Science and Engineering: A 375-377 (2004) 213

 218

^[2] B. Gludovatz, A. Hohenwarter, D. Catoor, E. H. Chang,

E. P. George, R. O. Ritchie, A fracture-resistant highentropy alloy for cryogenic applications, Science 345 (2014) 1153–1158.

^[3] Z. Zhang, M. M. Mao, J. Wang, B. Gludovatz, Z. Zhang, S. X. Mao, E. P. George, Q. Yu, R. O. Ritchie, Nanoscale

- origins of the damage tolerance of the high-entropy alloy crmnfeconi, Nature Communications 6 (2015) 10143.
- [4] S. Chen, H. S. Oh, B. Gludovatz, S. J. Kim, E. S. Park, Z. Zhang, R. O. Ritchie, Q. Yu, Real-time observations of trip-induced ultrahigh strain hardening in a dual-phase crmnfeconi high-entropy alloy, Nature Communications 11 (2020) 826.
- [5] Z. Wu, H. Bei, G. Pharr, E. George, Temperature dependence of the mechanical properties of equiatomic solid solution alloys with face-centered cubic crystal structures, Acta Materialia 81 (2014) 428 441.
- [6] Z. Zhang, H. Sheng, Z. Wang, B. Gludovatz, Z. Zhang, E. P. George, Q. Yu, S. X. Mao, R. O. Ritchie, Dislocation mechanisms and 3d twin architectures generate exceptional strength-ductility-toughness combination in crconi medium-entropy alloy, Nature Communications 8 (2017) 14390.
- [7] Q.-J. Li, H. Sheng, E. Ma, Strengthening in multiprincipal element alloys with local-chemical-order roughened dislocation pathways, Nature communications 10 (2019) 1–11.
- [8] R. Zhang, S. Zhao, J. Ding, Y. Chong, T. Jia, C. Ophus, M. Asta, R. O. Ritchie, A. M. Minor, Short-range order and its impact on the crconi medium-entropy alloy, Nature 581 (2020) 283–287.
- [9] B. Yin, S. Yoshida, N. Tsuji, W. Curtin, Yield strength and misfit volumes of nicocr and implications for shortrange-order, Nature Communications 11 (2020) 1–7.
- [10] W. Guo, Z. Pei, X. Sang, J. D. Poplawsky, S. Bruschi, J. Qu, D. Raabe, H. Bei, Shape-preserving machining produces gradient nanolaminate medium entropy alloys with high strain hardening capability, Acta Materialia 170 (2019) 176 – 186.
- [11] Z. Pei, An overview of modeling the stacking faults in lightweight and high-entropy alloys: Theory and application, Materials Science and Engineering: A 737 (2018) 132 – 150.
- [12] D. Ma, B. Grabowski, F. Körmann, J. Neugebauer, D. Raabe, Ab initio thermodynamics of the coerfemnni high entropy alloy: Importance of entropy contributions beyond the configurational one, Acta Materialia 100 (2015) 90 – 97.
- [13] F. Zhang, Y. Wu, H. Lou, Z. Zeng, V. B. Prakapenka, E. Greenberg, Y. Ren, J. Yan, J. S. Okasinski, X. Liu, Y. Liu, Q. Zeng, Z. Lu, Polymorphism in a high-entropy alloy, Nature Communications 8 (2017) 15687.
- [14] C. L. Tracy, S. Park, D. R. Rittman, S. J. Zinkle, H. Bei, M. Lang, R. C. Ewing, W. L. Mao, High pressure synthesis of a hexagonal close-packed phase of the high-entropy alloy crmnfeconi, Nature Communications 8 (2017) 15634.
- [15] F. X. Zhang, S. Zhao, K. Jin, H. Bei, D. Popov, C. Park, J. C. Neuefeind, W. J. Weber, Y. Zhang, Pressureinduced fcc to hcp phase transition in ni-based high entropy solid solution alloys, Applied Physics Letters 110 (2017) 011902.
- [16] C. Varvenne, A. Luque, W. A. Curtin, Theory of strengthening in fcc high entropy alloys, Acta Materialia 118 (2016) 164 – 176.
- [17] N. L. Okamoto, S. Fujimoto, Y. Kambara, M. Kawamura, Z. M. Chen, H. Matsunoshita, K. Tanaka, H. Inui, E. P. George, Size effect, critical resolved shear stress, stacking fault energy, and solid solution strengthening in the crmnfeconi high-entropy alloy, Scientific reports 6 (2016)

- 35863.
- [18] S. Wei, C. C. Tasan, Deformation faulting in a metastable cocrniw complex concentrated alloy: A case of negative intrinsic stacking fault energy?, Acta Materialia 200 (2020) 992 – 1007.
- [19] Z. Pei, G. M. Stocks, Origin of the sensitivity in modeling the glide behaviour of dislocations, International Journal of Plasticity 106 (2018) 48 – 56.
- [20] C. Niu, C. R. LaRosa, J. Miao, M. J. Mills, M. Ghazisaeidi, Magnetically-driven phase transformation strengthening in high entropy alloys, Nature Communications 9 (2018) 1363.
- [21] F. Zhang, Y. Ren, Z. Pei, Z. Lu, B. Wang, Y. Xue, X. Cao, K. Du, Y. Yang, B. Li, M. Chen, Dislocation cooperation for hierarchical deformation in shock-loaded multi- principal element alloys, submitted (2021).
- [22] X. Xu, P. Liu, Z. Tang, A. Hirata, S. Song, T. Nieh, P. Liaw, C. Liu, M. Chen, Transmission electron microscopy characterization of dislocation structure in a face-centered cubic high-entropy alloy alo. 1cocrfeni, Acta Materialia 144 (2018) 107–115.
- [23] K. Lagerlöf, J. Castaing, P. Pirouz, A. Heuer, Nucleation and growth of deformation twins: a perspective based on the double-cross-slip mechanism of deformation twinning, Philosophical Magazine A 82 (2002) 2841–2854.
- [24] J. P. Hirth, J. Lothe, Theory of dislocations (Ed.2), Krieger Publishing, Malabar, UK, 1992.
- [25] M. Chen, E. Ma, K. J. Hemker, H. Sheng, Y. Wang, X. Cheng, Deformation twinning in nanocrystalline aluminum, Science 300 (2003) 1275–1277.
- [26] G. P. M. Leyson, W. A. Curtin, L. G. Hector, C. F. Woodward, Quantitative prediction of solute strengthening in aluminium alloys, Nature materials 9 (2010) 750–755.
- [27] D. Ma, M. Friák, J. von Pezold, D. Raabe, J. Neugebauer, Computationally efficient and quantitatively accurate multiscale simulation of solid-solution strengthening by ab initio calculation, Acta Materialia 85 (2015) 53 – 66.
- [28] Z. Pei, D. Ma, M. Friák, B. Svendsen, D. Raabe, J. Neugebauer, From generalized stacking fault energies to dislocation properties: Five-energy-point approach and solid solution effects in magnesium, Phys. Rev. B 92 (2015) 064107.
- [29] S. Sandiöbes, M. Friák, S. Zaefferer, A. Dick, S. Yi, D. Letzig, Z. Pei, L.-F. Zhu, J. Neugebauer, D. Raabe, The relation between ductility and stacking fault energies in mg and mg-y alloys, Acta Materialia 60 (2012) 3011 – 3021.
- [30] Q.-M. Hu, R. Yang, Basal-plane stacking fault energy of hexagonal close-packed metals based on the ising model, Acta Materialia 61 (2013) 1136 – 1145.
- [31] G. Schoeck, The Peierls model: Progress and limitations, Materials Science and Engineering: A 400-401 (2005) 7 – 17. Dislocations 2004.
- [32] G. Leibfried, H. D. Dietze, Versetzungsstrukturen in kubisch-flächenzentrierten kristallen. i, Zeitschrift für Physik 131 (1951) 113–129.
- [33] X. Liu, Z. Pei, M. Eisenbach, Dislocation core structures and peierls stresses of the high-entropy alloy nicofecrmn and its subsystems, Materials & Design 180 (2019) 107955.
- [34] Z. Pei, S. Mu, W. Ming, The local strain distribution in bilayer materials: a multiscale study, Nanoscale 12

- (2020) 6456-6461.
- [35] Z. Pei, M. Eisenbach, Acceleration of the particle swarm optimization for Peierls-Nabarro modeling of dislocations in conventional and high-entropy alloys, Computer Physics Communications 215 (2017) 7 – 12.
- [36] Z. Pei, Dist: A dislocation-simulation toolkit, Computer Physics Communications 233 (2018) 44 – 50.
- [37] B. Yin, W. A. Curtin, First-principles-based prediction of yield strength in the RhIrPdPtNiCu high-entropy alloy, npj Computational Materials 5 (2019) 1–7.
- [38] W. G. Nöhring, W. Curtin, Correlation of microdistortions with misfit volumes in high entropy alloys, Scripta Materialia 168 (2019) 119 – 123.
- [39] S. S. Nene, M. Frank, K. Liu, R. S. Mishra, B. A. McWilliams, K. C. Cho, Extremely high strength and work hardening ability in a metastable high entropy alloy, Scientific Reports 8 (2018) 9920.
- [40] Z. Wang, W. Lu, D. Raabe, Z. Li, On the mechanism of extraordinary strain hardening in an interstitial high-

- entropy alloy under cryogenic conditions, Journal of Alloys and Compounds 781 (2019) 734 743.
- [41] S. Picak, J. Liu, C. Hayrettin, W. Nasim, D. Canadinc, K. Xie, Y. Chumlyakov, I. Kireeva, I. Karaman, Anomalous work hardening behavior of fe40mn40cr10co10 high entropy alloy single crystals deformed by twinning and slip, Acta Materialia 181 (2019) 555 – 569.
- [42] X. Gao, Y. Lu, J. Liu, J. Wang, T. Wang, Y. Zhao, Extraordinary ductility and strain hardening of Cr26Mn20Fe20Co20Ni14 twip high-entropy alloy by cooperative planar slipping and twinning, Materialia 8 (2019) 100485.
- [43] G. Dieter, Mechanical metallurgy, McGraw-Hill Higher Education, 1986.
- [44] A. Tirunilai, T. Hanemann, K.-P. Weiss, J. Freudenberger, M. Heilmaier, A. Kauffmann, Dislocation-based serrated plastic flow of high entropy alloys at cryogenic temperatures, Acta Materialia 200 (2020) 980 991.